Eur Biophys J (2010) 39:935–945
DOI 10.1007/s00249-009-0459-4

ORIGINAL PAPER

Identifying the structure of the active sites of human recombinant prolidase

Roberta Besio · Stefania Alleva · Antonella Forlino · Anna Lupi · Carlo Meneghini · Velia Minicozzi · Antonella Profumo · Francesco Stellato · Ruggero Tenni · Silvia Morante

Received: 26 January 2009 / Revised: 26 March 2009 / Accepted: 7 April 2009 / Published online: 5 May 2009

Abstract In this paper we provide a detailed biochemical and structural characterization of the active site of recombinant human prolidase, a dimeric metalloenzyme, whose misfunctioning causes a recessive connective tissue disorder (prolidase deficiency) characterized by severe skin lesions, mental retardation and respiratory tract infections. It is known that the protein can host two metal ions in the active site of each constituent monomer. We prove that two different kinds of metals (Mn and Zn) can be simultaneously present in the protein active sites with the protein partially maintaining its enzymatic activity. Structural information extracted from X-ray absorption spectroscopy measurements have been used to yield a full reconstruction of the atomic environment around each one of the two monomeric active sites. In particular, as for the metal ion occupation configuration of the recombinant human prolidase, we have found that one of the two active sites is occupied by two Zn ions and the second one by one Zn and one Mn ion. In both dinuclear units a histidine residue is bound to a Zn ion.

Keywords Human recombinant prolidase · X-ray absorption spectroscopy · Site structure

Abbreviations

APPro	Aminopeptidase proline
Asp	Aspartic acid
DESY	Deutsches Elektronen-Synchrotron
DTT	Dithiothreitrol
DW	Debye–Waller
EMBL	European Molecular Biology Laboratory
EXAFS	Extended X-ray absorption fine structure
FT	Fourier transform
Glu	Glutamic acid
Gly	Glycine
His	Histidine
ICP-MS	Inductively coupled plasma-mass spectrometry
MetAP	Methionine aminopeptidase
MS	Multiple scattering
PDB	Protein Data Bank
PEPD	Peptidase D: prolidase gene
Pfprol	*Pyrococcus furiosus* prolidase
XAS	X-ray absorption spectroscopy
Pro	Proline
XANES	X-ray absorption near edge structure

Introduction

Human prolidase is the only metalloenzyme among the peptidases that cleaves the iminodipeptides containing a proline or hydroxyproline residue at the C-terminal end. It

Proceedings of the XIX Congress of the Italian Society of Pure and Applied Biophysics (SIBPA), Rome, September 2008.
S. Alleva is the co-first author.

R. Besio · A. Forlino · A. Lupi · R. Tenni
Dipartimento di Biochimica Sez. Medicina e Farmacia, Università di Pavia, Pavia, Italy

S. Alleva · V. Minicozzi · F. Stellato · S. Morante (✉)
Dipartimento di Fisica and INFN, Università di Roma "Tor Vergata", Rome, Italy
e-mail: morante@roma2.infn.it

C. Meneghini
Dipartimento di Fisica, Università di Roma Tre, Rome, Italy

A. Profumo
Dipartimento di Chimica, Università di Pavia, Pavia, Italy

requires Mn(II) and reducing conditions for full activity, at least in in vitro assay. It is relevant in the latest stages of protein catabolism, particularly of those molecules rich in iminoacids such as collagens, thus it turns out to be involved in matrix remodeling (Royce and Steinmann 2002). Mutations in the prolidase gene (PEPD) cause prolidase deficiency, a rare autosomal recessive connective tissue disorder characterized by intractable skin lesion, mental retardation and respiratory tract infections (Lupi et al. 2008).

Currently, the majority of prolidase proteins that have been studied are metalloenzymes, requiring divalent cations such as Zn(II), Mn(II) or Co(II) in their active sites. They have been purified either as monomers or as dimers depending on the enzyme (Wilcox 1996; Lowther and Matthews 2002; Cunningham and O'Connor 1997; Kobayashi and Shimizu 1999; Yang and Tanaka 2008). Their main activity is X-Pro dipeptides hydrolysis, although some prolidase proteins were found to be able to cleave dipeptides with proline at the N-terminal end or dipeptides that do not contain a proline residue (Browne and O'Cuinn 1983; Fernandez-Espla et al. 1997; Fujii et al. 1996). The variability of substrate specificity can depend on the numbers of subunits present in the active enzyme as well as on the nature of the metal ion occupying the active site.

The structure of human prolidase, as well as the geometry of its active site and the catalytic mechanism, is still poorly understood. Besides data extrapolated from comparative studies on prolidase from other organisms, recently the 3D structure of human prolidase has been solved. Two structures are, in fact, deposited in PDB, one with Na(I) (PDB ID: 2iw2) and the other one with Mn(II) (PDB ID: 2okn) in the active site. It should be said, however, that to our knowledge the corresponding papers have not yet been published.

The best characterized prolidase in terms of structure and catalytic site composition is the one isolated from the archaeon *Pyrococcus furiosus* recombinantly produced in *E. coli* (Du et al. 2005). *P. furiosus* prolidase (Pfprol) displays a 28% identity with human prolidase. Like the human enzyme, it is a homodimer with two subunits. Each monomer has a dinuclear metal cluster requiring Co(II) for full activity. It should be immediately noted that in the crystallization process, Zn(II) ions substituted native Co(II) ions (Maher et al. 2004). Furthermore, only data for one of the two Pfprol monomers are available, as the second monomer remained seriously disordered.

There also exists full crystallographic data on the 3D structure of the prolidase from the related *P. horikoshii OT3* archeon (PDB ID: 1wy2) (about 28% identity with human enzyme and 80% identity with Pfprol). For this reason we have used the latter to set up a reliable ansatz for the geometrical model of the protein active site when fitting our extended X-ray absorption fine structure (EXAFS) data (see below).

From the analysis of the available X-ray crystallographic structure of *P. horikoshii OT3* five amino acids have been identified as metal-binding residues. They are His287, Glu316, Asp212, Asp223 and Glu330. In human prolidase the corresponding amino acids turn out to be His371, Glu413, Asp277, Asp288 and Glu453. The fact that Glu413, Asp277, Glu453 are relevant for structural stability and activity of human prolidase is demonstrated by the molecular characterization of prolidase deficiency patients with mutations at these amino acid sites (Lupi et al. 2008).

The mechanism of prolidase catalysis is still largely unknown. However, prolidase belonging to the "pita-bread" enzyme family together with MetAP and APPro (Roderick and Matthews 1993; Maher et al. 2004) allowed Lowther and Matthews (2002) to propose a common reaction mechanism. Indeed, all these enzymes are able to cleave amido-, imido- and amidino-containing peptides bonds, exhibiting relatively narrow substrate specificities when compared to the other metalloaminopeptidases. They contain in the active sites dinuclear metal clusters coordinated by identical sets of amino acidic residues (i.e., two Glu, two Asp and one His) with the metal bound to the His residue showing the highest affinity (Tahirov et al. 1998). There is evidence (D'souza et al. 2000; Cosper et al. 2001), however, that at variance with the human and *Pyrococcus* prolidases (Du et al. 2005), prokaryotic MetAP is active when only one metal ion is bound to the dinuclear cluster of each monomer, while the activity decreases when full occupation is achieved.

Few years ago, Lupi et al. synthesized the human prolidase in prokaryotic and eukaryotic hosts, and showed that the recombinant enzyme has molecular weight (57 kDa), optimal pH (pH 7.8) and optimal temperature (50°C) activity, as well as metal requirement (Mn) for full activity identical to the endogenous human fibroblasts prolidase. They also demonstrated that the thermal stability of recombinant and endogenous enzyme were similar (Lupi et al. 2006).

In the present study, the recombinant enzyme produced in *E. coli* is used to investigate the enzyme active sites composition and structure with the help of X-ray absorption spectroscopy (XAS).

Materials and methods

Sample preparation and characterization

Recombinant human prolidase was produced in BL21 *E. coli* cells as fusion protein with an N-terminal His tag

and purified, upon Mn(II) preactivation for 1 h at 50°C, using affinity chromatography, as described in Lupi et al. (2006). Following enzymatic removal of the tag by means of on-column Factor Xa digestion, the protein was extensively dialyzed against 10 mM Tris–HCl pH 7.8, 0.57 mM dithiothreitrol (DTT) and 300 mM NaCl.

Two different protein preparations, purified independently from glycerol stock of transformed bacteria, were obtained for the successive XAS study, referred to as P1 and P2 in this work. The two independent preparations were concentrated by a quick dialysis against PEG 20000 to reduce the sample volume to 100 µl keeping the protein in solution. Protein concentration was determined by the method of Lowry et al. (1951) using bovine serum albumin as standard. Taking into account that the recombinant enzyme is obtained mainly in dimeric form, as determined by gel filtration chromatography (Lupi et al. 2008), the two different protein preparation solutions, P1 and P2, were found to have a concentration of (32 ± 3) µM and (78 ± 8) µM, respectively (see Table 1).

The amount of divalent metals present in solution was measured using inductively coupled plasma-mass spectrometry (ICP-MS) on a Perkin Elmer Mod. ELAN DRC-e instrument, following the standard procedures suggested by the manufacturer.

The enzymatic activity is evaluated according to the method proposed by Myara et al. (1982). A quantity ranging from 6 to 8 × 10^{-4} mg ml^{-1} of purified enzyme dissolved in 50 µl of 50 mM Tris–HCl, pH 7.8 is incubated for 1 h at 50°C in the presence of 0.75 mM of reduced glutathione, 100 mM Gly-Pro, and in the presence of different concentrations of $MnCl_2$ (0.00, 0.05, 0.5, 1, 5, 10 mM). At this point, acetic acid and Chinard's Reagent (Chinard 1952) are added and the mixture incubated for 10 min at 90°C. Spectrophotometric measurements are performed at 515 nm and the activity is expressed as µmol of Pro residue hydrolyzed per hour and mg of protein. The activity has also been measured in the presence of different concentrations of $ZnCl_2$ (0.00, 0.05, 0.5, 1, 10, 50 mM).

Table 1 Protein and metal concentrations of preparations MeP1 and MeP2 (Me = Mn/Zn)

	[Protein] µM	[Mn(II)]	[Zn(II)]
MeP1	(32 ± 3)	(28 ± 3) µM	(90 ± 10) µM
[P1]:[metal]		~1:1	~1:3
MeP2	(78 ± 8)	(55 ± 6) µM	(750 ± 70) µM
[P2]:[metal]		~1:1	~1:10
MnB		2 mM	
ZnB			2 mM

In the last two rows we give the concentration of the metal, Mn or Zn, added to the blank, namely the buffer used to perform dialysis

X-ray absorption spectroscopy

X-ray absorption spectroscopy data have been collected at the D2 bending magnet beam line of the EMBL Outstation Hamburg at DESY. The synchrotron was operating at 4.5 GeV with ring currents ranging from 90 to 149 mA. A Si[111] double crystal monochromator and a focusing mirror with a cut-off energy of 21.5 KeV have been used. Spectra were recorded in fluorescence mode using a 13-element Ge solid-state detector (Canberra, Meriden, CT, USA). The samples were kept at 20 K in a He close-cycle cryostat (Oxford Instruments) throughout the whole measurement session. Upon measurement, 25 µl of each sample is transferred in a 1-mm thick plastic holder closed by two Kapton® windows, rapidly frozen in liquid nitrogen and immediately brought to the experimental hutch.

XAS data analysis

For each sample several (from 34 to 47) XAS spectra have been collected and averaged. After background subtraction, the resulting spectrum was normalized using the Kemp software (Korbas et al. 2006) and the spectroscopic signal extracted using the Athena software (Ravel and Newville 2005).

Extended X-ray absorption fine structure data have been analyzed using the FITEXA software (see the Appendix and http://webusers.fis.uniroma3.it/~meneghini/ for details), where the theoretical absorption coefficient is calculated by taking into account single and multiple scattering (MS) contributions. In the fitting procedure the experimental data are weighted by a factor k (Teo and Lee 1979) to compensate for their rapid decrease with increasing k.

Results and discussion

The work we present here provides the first experimental evidence for the coexistence of two kinds of ions in the active site of human prolidase, without complete loss of the protein enzymatic activity.

In the literature it is almost generally accepted (see for instance Du et al. 2005; Maher et al. 2004; Royce and Steinmann 2002) that the presence of Zn in the active site significantly reduces prolidase activity. Actually, there are also indirect evidences that in prolidase the binding site is not terribly selective against the nature of the bonded divalent ion. A typical case in this respect is Pfprol where in the crystal Zn(II) substitutes Co(II), supposedly necessary for full enzymatic activity.

In this paper we have been able to demonstrate that two different kinds of metal ions [Mn(II) and Zn(II) in this

instance] can be simultaneously present in the dinuclear binding site of human prolidase with the protein remaining partially active.

Enzymatic activity

The specific enzymatic activity was measured with no further addition of both Mn and Zn ions and found to be $(2.3 \pm 0.7) \times 10^3$ μmol proline h^{-1} mg^{-1}. Activity was also measured in excess (10 mM) of either Mn or Zn. At such a high concentration we can assume that all the four active sites are homogeneously loaded with Mn or Zn, respectively. At 10 mM $MnCl_2$ the specific activity was 9,500 ± 7 μmol proline h^{-1} mg^{-1}, while at 10 mM $ZnCl_2$ was 800 ± 40 μmol $proline^{-1}$ h^{-1} mg, These values are about four times higher and three times lower than basal activity, respectively.

Metal ions content

As recalled in "Sample preparation and characterization", the metal ion concentration of the two (P1 and P2) samples was determined using ICP-MS. The results of these measurements are reported in Table 1 together with the corresponding protein concentration. It was found that a large amount of Zn(II) was present in both preparations probably originating from the Zn ions present into bacteria cells.

Indeed, we see from Table 1 that, while the ratio protein over Mn(II) concentration[1] is about 1:1 for both samples, the ratio protein over Zn(II) is 1:3 in sample P1 and much larger, reaching the value 1:10, in sample P2.

Recalling that each protein molecule can host at most four metal ions in the active sites (there is a dinuclear site for each of the two monomers), we may interpret the numbers in Table 1 by saying that in the case of sample P1 the totality of the available metal ions [namely Zn(II) and Mn(II)] is bound to the protein. On the contrary, in the case of sample P2 we expect to have a Zn(II) excess free in solution.

As we will show later, XAS spectral data properly confirm the relative metal abundances reported in Table 1 and furthermore provide evidence that indeed the Zn(II) excess present in sample P2 is free in solution.

XAS

X-ray absorption spectroscopy spectra are analyzed by separating the near edge region, the so-called X-ray near edge structure (XANES) region, which extends from few eV below the edge energy to about 50 eV above, from the comparatively higher energy EXAFS region which extends from about 50 eV above the edge onward.

The reason for this separation is that the theoretical interpretation of the structural features visible in the XANES region of the spectrum is rather delicate and difficult, because in this low-energy range the shape of the spectrum is determined by many complicated electronic processes (Lee and Pendry 1975; Benfatto et al. 1986; Gurman et al. 1986; Koningsberger and Prins 1988; Rehr and Albers 1990) and it turns out to be very sensitive to the electronic structure of the absorber and the symmetry of the local environment around it (Bianconi et al. 1986). Consequently, the XANES region is normally used to get only qualitative structural information. At variance, the EXAFS region (Meneghini and Morante 1998) can provide valuable quantitative geometrical information about the structure of the absorber environment.

We remark immediately that in order to have a good signal-to-noise ratio out of the four XAS spectra we collected (samples P1 and P2 at both the Mn and Zn K-edge) we decided to subject the samples to a detailed analysis and theoretical fit only the data taken on sample P1 at the Zn K-edge (owing to the absence of free Zn in solution) and on sample P2 at the Mn K-edge (owing to the sufficiently high absorber concentration).

The buffer in which protein is dissolved, namely 10 mM Tris–HCl, pH 7.8, 0.57 mM DTT and 0.3 M NaCl has been also subjected to XAS measurement both in presence of 2 mM $MnCl_2$ (MnB) and of 2 mM $ZnCl_2$ (ZnB). These two samples have been used to check the difference between the structure of the metal free in solution (in buffer in the absence of the protein) and bound to the protein.

XANES

Despite the difficulties mentioned above, a qualitative comparison of XANES spectra of prolidase samples with the corresponding metal in buffer is useful and shows significant structural differences both at the Mn (Fig. 1a) and Zn (Fig. 1b) K-edge. It is particularly interesting to notice that at the Zn K-edge the P2 sample spectrum (from now on ZnP2 for short) displays features somehow in between those characteristic of sample P1 (ZnP1) and the buffer solution (ZnB). This observation gives support to the very reasonable working hypothesis we already mentioned, that the Zn excess in sample P2 is free in solution. Indeed one can check that, if we can assume that in sample P1 all the available Zn is instead bound at the protein active sites, then the ZnP2 spectrum can be understood as a simple superposition of the ZnP1 and ZnB spectra. Further support to this conclusion comes from a semi-quantitative analysis of the EXAFS region of the ZnP2 spectrum (see below and Fig. 2).

[1] The weight of the recombinant dimeric prolidase is 123,600 Da (Lupi et al. 2008).

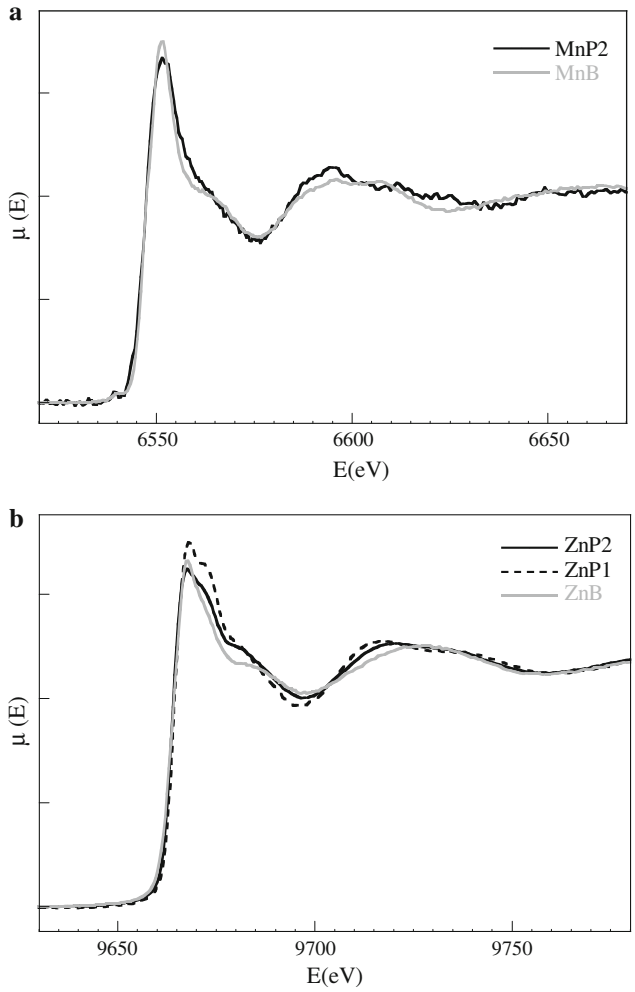

Fig. 1 **a** Comparison of the XANES spectra at the Mn K-edge of sample P2 (MnP2, *black line*) and buffer (MnB, *gray line*). We do not plot the much too noisy MnP1 spectrum. **b** Comparison of the XANES spectra at the Zn K-edge of sample P2 (ZnP2, *full black line*), P1 (ZnP1, *broken black line*), and buffer (ZnB, *gray line*)

EXAFS

Before going into the details of the analysis of the EXAFS signal, $\chi(k)$,[2] two premises are necessary:

1. First of all we need to justify the choice we made to limit our analysis of the EXAFS region to sample P1 at the Zn K-edge.
2. Secondly, we want to give a detailed description of the geometrical model of the metal environments we will take as starting atomic configurations for our fits to the EXAFS data.

For what concerns point (1), as already suggested in the previous paragraph, the ZnP2 EXAFS spectrum appears to

[2] The relation between the measured absorption coefficient, $\mu(E)$, and the derived signal $\chi(k)$ is given in Appendix.

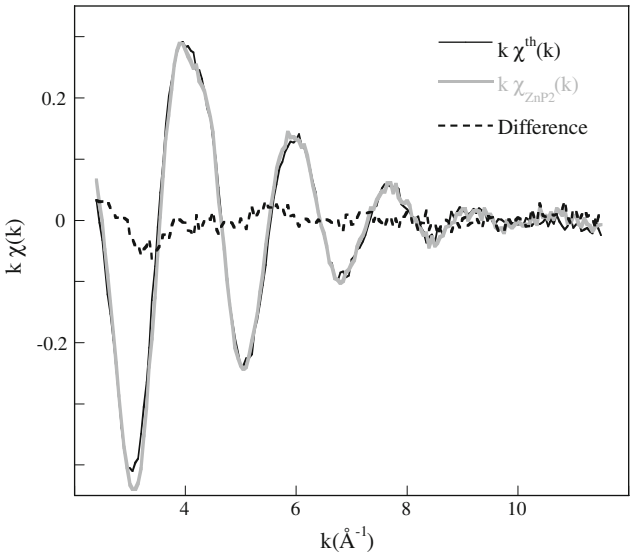

Fig. 2 Experimental spectrum $k\chi_{\mathrm{ZnP2}}(k)$ (in *gray*) superimposed to$k\chi^{\mathrm{th}}(k)$ (in *black*) computed at the best fit value$\bar{\alpha} = (44 \pm 8)\%$. The *broken line* is their difference

be the sum of two distinct contributions, one from the bound Zn (as in sample P1) and the other from Zn free in buffer. It is then natural to try a quantitative estimate of the relative weight of the two contributions by setting

$$\chi^{\mathrm{th}}(k) = \alpha\chi_{\mathrm{ZnP1}}(k) + (1-\alpha)\chi_{\mathrm{ZnB}}(k) \tag{1}$$

where α is determined by minimizing the objective function

$$F(\alpha) = \sum_k k^2 \left|\chi_{\mathrm{ZnP2}}(k) - \chi^{\mathrm{th}}(k)\right|^2 = \sum_k k^2 |\chi_{\mathrm{ZnP2}}(k) - \alpha\chi_{\mathrm{ZnP1}}(k) - (1-\alpha)\chi_{ZnB}(k)|^2. \tag{2}$$

In Eq. 2, the sum over k is extended over all the value of the photon momentum at which data were taken. For best fit value one finds $\bar{\alpha} = (44 \pm 8)\%$. Figure 2 summarizes the result of the minimization. In figure, the experimental spectrum, $k\chi_{\mathrm{ZnP2}}(k)$, is drawn in gray superimposed to $k\chi^{\mathrm{th}}(k) = k[\bar{\alpha}\chi_{\mathrm{ZnP1}}(k) + (1-\bar{\alpha})\chi_{\mathrm{ZnB}}(k)]$, in black. The broken line is the difference $k\left[\chi_{\mathrm{ZnP2}}(k) - \chi^{\mathrm{th}}(k)\right]$.

Interestingly enough, even such a rough analysis ends with a nice quantitative result, which within the estimated error on $\bar{\alpha}$ is compatible with the hypothesis that in the P2 sample about two-third of the whole amount of Zn is free in solution (see Table 1).

At this point we decided to limit the analysis of the EXAFS data at the Zn K-edge, to the ZnP1 spectrum where all the Zn is supposed to be bound to the protein active sites.

As it is always the case in the EXAFS analysis, the requirement of having a realistic geometrical model around

the absorber to go on with the fitting procedure is a crucial prerequisite for the reliability of the derived structural information. In the case at hand, even after excluding the situation in which one has free Zn in solution, we still have the problem that the four metal binding sites are not all structurally identical. Thus, there is site heterogeneity which makes the search for realistic metal coordination modes absolutely mandatory.

A standard way to try to cope with this situation is to exploit the information available in the Protein Data Bank (PDB) (Berman et al. 2000), where structures of prolidase expressed in various organisms and in complex with different metal ions are collected. It should, however, be kept in mind that, as already said in "Introduction", among the deposited prolidase structures none is found to be simultaneously in complex with two different types of metal ions, unlike the situation we are interested in this paper. Lacking this peculiar heterogeneous structure among the available crystallographic data, we chose to build our starting model using complementary geometrical information coming from the following two proteins:

1. Human prolidase in complex with Mn(II) (PDB ID: 2okn);
2. *P. horikoshii OT3* prolidase in complex with Zn (II) (PDB ID: 1wy2).[3]

The 3D structure of these two complexes yields good models for the Mn and Zn coordination mode, respectively. In both cases the protein is a dimer made of two identical monomers (identified as monomer 1 and monomer 2 in the following) and each monomer can host two metal ions in two structurally distinct binding sites (that we call site A and site B, respectively; see Fig. 3). In each protein molecule there are, therefore, four distinct metal binding sites that are indicated by A1 and A2 (highlighted in green) and B1 and B2 (highlighted in magenta) in Fig. 3.

In Table 2 we outline the PDB metal coordination modes of the two selected structures. We report type and number of atoms bound to the corresponding metal ion in the four different sites. At this stage it is not necessary to specify which amino acid residue the reported oxygen atoms belong to. It is, however, important to remark that the sites of type A, where a His residue is one of the ligands, are structurally very different from the sites of type B where only light scatterers (typically oxygen) are coordinated to the metal. We also observe that the metal coordination mode in sites A1 and A2 are identical in the crystallographic structure of human prolidase and *P. horikoshii OT3*, while the strict equality of B sites only holds for the 1wy2 (Zn) complex.

Relying on the observation that concentration ratio between protein and Mn(II) measured in our samples is 1:1 (see Table 1), we may safely assume that out of the four prolidase binding sites one is occupied by a Mn(II) ion and the remaining ones by three Zn(II) ions. Thus the four combinations of metal occupations shown in Table 3 are possible. Actually only two of them (S_1 and S_2) are significantly different. In fact, as remarked above in the discussion of Table 2, the site environments S'_2 and S_2 are just identical (as explicitly indicated in Table 3) because the Mn coordination modes in sites A1 and A2 are identical. The site environments S_1 and S'_1 are instead not exactly equal. They differ because (see Table 2) in S_1 Mn is coordinated to five oxygens (site B1), while in S'_1 it is coordinated to six oxygens (site B2).

Fit at the Mn K-edge

The fit at the Mn K-edge was carried out using the MnP2 EXAFS data because, as we said, the Mn (and the protein) concentration in sample P1 (see Table 1) turned out to be too low to yield a sufficiently good experimental signal-to-noise ratio.

Since the protein to metal concentration ratio is 1:1, the $\chi_{\mathrm{MnP2}}(k)$ EXAFS signal is fitted assuming that the Mn(II) coordination mode is unique and structurally of the kind one finds in the 2okn complex, as reported in Table 2. We thus decided to try as starting models for fitting our data the 3D structures of the three different Mn sites (A1 $\equiv$ A2) listed in the first row of Table 2, appropriately modified to host an extra Zn(II) ion next to the Mn(II) absorber.

Among the configurations listed in Table 3, the one that gives rise to the best fit is S'_1 where Mn(II) is located in the B2 site. The quality factor of the fit is rather good giving $R^2 = 11\%$ (see Appendix for the definition of R^2). For comparison we notice that we get the larger value $R^2 = 15\%$ if Mn(II) is assumed to be located in the B1 or the A1 $\equiv$ A2 site.

The experimental signal (gray line) and the theoretical fit (black line) are plotted in Fig. 4 (upper panel) together with the corresponding Fourier transform (FT, lower panel). The structural parameters of the best fit are reported in Table 4. In the first and second column we display type and number, N, of scatterers. In the third and fourth column we report the distance, r, of the absorber from the corresponding (shell of) scatterers and the associated Debye–Waller factors, σ^2_{DW}. Errors are statistical and are written next to each parameter. The Fermi energy shift, E_{F}, and the quality factor, R^2, of the fit are reported in the last row. The physical meaning of the parameters listed in Table is briefly described in the Appendix.

[3] As already commented in "Introduction," we indicated that we have decided to employ the 3D crystallographic data of *P. horikoshii OT3* as for the latter (unlike *P. furiosus*) both monomers have been resolved.

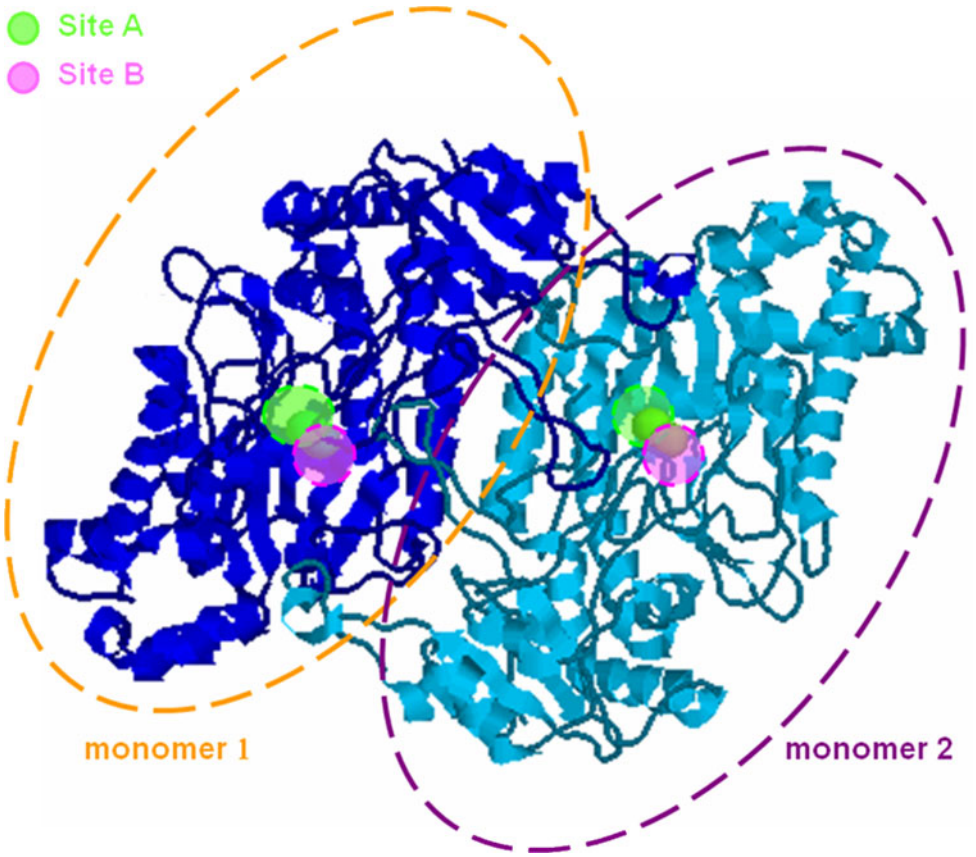

Fig. 3 A cartoon of the prolidase dimer. Sites A are highlighted in *green* and sites B in *magenta*. The crystal structure of human recombinant prolidase (PDB ID: 2iw2) is used for the sketch

Table 2 Metal coordination mode at the A1, B1, A2, B2 sites in the 2okn and 1wy2 complexes

Complexes	A1	B1	A2	B2
2okn (Mn)	4O,1 N_{ε}(His)	5O	4O,1 N_{ε}(His)	6O
1wy2 (Zn)	4O,1 N_{ε}(His)	4O	4O,1 N_{ε}(His)	4O

Table 3 The four possible metal occupations of sites A1, B1, A2, B2

	Monomer 1		Monomer 2	
	A1	B1	A2	B2
S_1	Zn	Mn	Zn	Zn
S_2	Mn	Zn	Zn	Zn
S'_1	Zn	Zn	Zn	Mn
$S'_2 = S_2$	Zn	Zn	Mn	Zn

Fit at the Zn K-edge

We now move to analyze the data collected at the Zn K-edge. We recall that, given the large amount of Zn in solution in sample P2, we have been forced to use the ZnP1 spectral data to investigate the structure of the Zn(II) coordination mode. Exploiting the information we gathered from the previous fit (i.e., that Mn is in the B2 site), we can assume that the three Zn(II) ions occupy the sites A1, A2 and B1. In this situation the measured EXAFS signal at the Zn K-edge will be the sum of three contributions: one, $\chi_{A1}(k)$, in which the photo-electron is extracted from the Zn(II) ion sitting in site A1 [another Zn(II) ion sits nearby in site B1], a second contribution, $\chi_{B1}(k)$, where the extracted photo-electron belongs to the Zn(II) ion located in site B1 [as before another Zn(II) ion sits nearby in site A1] and a third one, $\chi_{A2}(k)$, in which the extracted photo-electron comes from the Zn(II) ion located in site A2 [this time among the near scatterers there is a Mn(II) ion sitting in site B2]. We thus write

$$\chi_{ZnP2}(k) = \frac{1}{3}[\chi_{A1}(k) + \chi_{A2}(k) + \chi_{B1}(k)]. \quad (3)$$

In Table 5, we summarize the results of the best fit, listing the geometrical parameters that characterize the three Zn binding sites. As one can see from the very small value of R^2 ($R^2 = 3\%$), the fit is extremely good. In Fig. 5, we show the experimental signal (gray line) with superimposed the theoretical (black line) spectrum (upper panel) as well as their FT's (lower panel). A cartoon of the geometries of the four prolidase metal binding sites is sketched in Fig. 6.

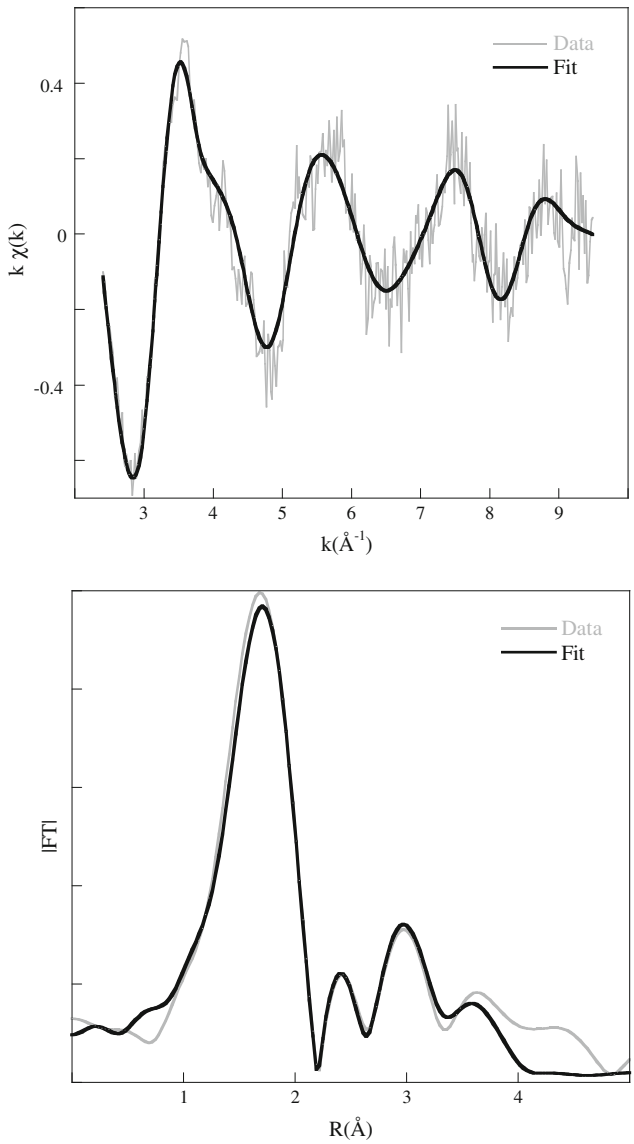

Fig. 4 Experimental data (*gray line*) and theoretical fit (*black line*) at the Mn K-edge. In the *upper panel* we show the EXAFS signals and in the *lower panel* the corresponding FT's

Table 4 Best fit parameters from the MnP2 spectrum

Type of scatterer	N	$(r \pm \Delta r)$ Å	$(\sigma^2_{DW} \pm \Delta\sigma^2_{DW})$ 10^{-3} Å^2
O	6	2.23 ± 0.01	1.1 ± 0.5
Zn	1	3.40 ± 0.01	1.2 ± 1.0

$\Delta E_F = (16.7 \pm 0.4)$ eV, $R^2 = 11\%$

Conclusions

With a combined use of ICP-MS and XAS measurements we have been able to provide a tight biochemical and structural characterization of human prolidase showing for the first time the existence of heterogeneous dimeric metallic sites in the active form of the protein. We have seen, in fact, that, even in the presence of over-concentrated Zn(II) ions, the protein partially retains its enzymatic

Table 5 Best fit parameters from the ZnP2 spectrum

Site	Type of scatterer	N	$(r \pm \Delta r)$ Å	$(\sigma^2_{DW} \pm \Delta\sigma^2_{DW})$ 10^{-3} Å^2
A1	O	4	2.05 ± 0.01	1.5 ± 0.4
	N_ε	1	2.05 ± 0.01	1.5 ± 0.4
	Zn	1	3.21 ± 0.04	2.3 ± 1.5
A2	O	4	2.05 ± 0.01	1.5 ± 0.4
	N_ε	1	2.05 ± 0.01	1.5 ± 0.4
	Mn	1	3.37 ± 0.03	2.3 ± 1.5
B2	O	4	1.90 ± 0.01	1.5 ± 0.4
	Zn	1	3.21 ± 0.04	2.3 ± 1.5

$\Delta E_F = (14.2 \pm 0.1)$ eV, $R^2 = 3\%$

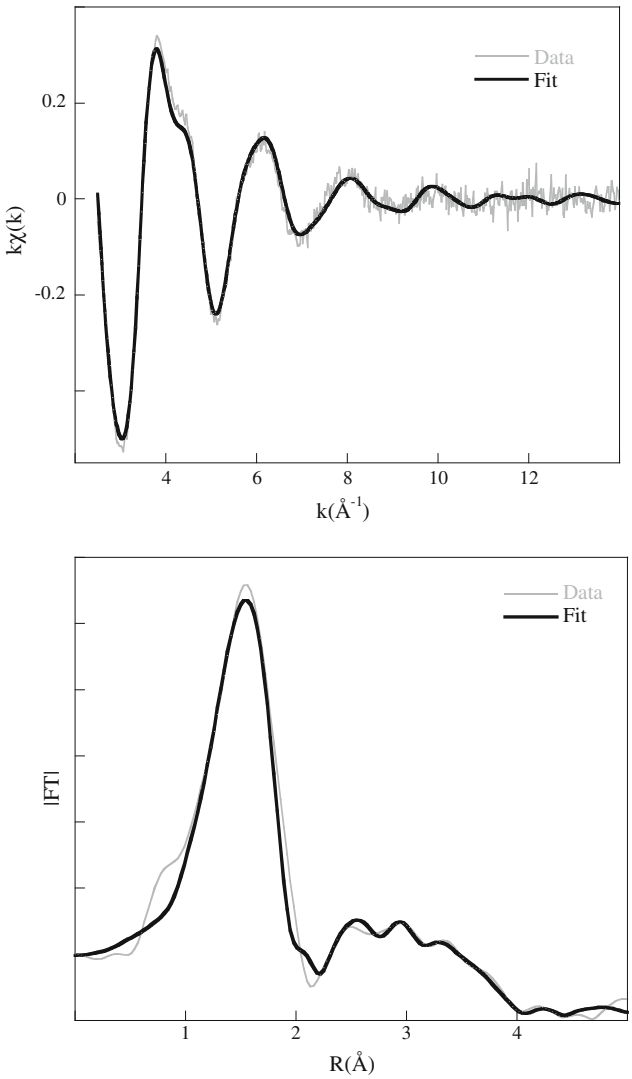

Fig. 5 Experimental data (*gray line*) and theoretical fit (*black line*) at the Zn K-edge. In the *upper panel* we show the EXAFS signals and in the *lower panel* the corresponding FT's

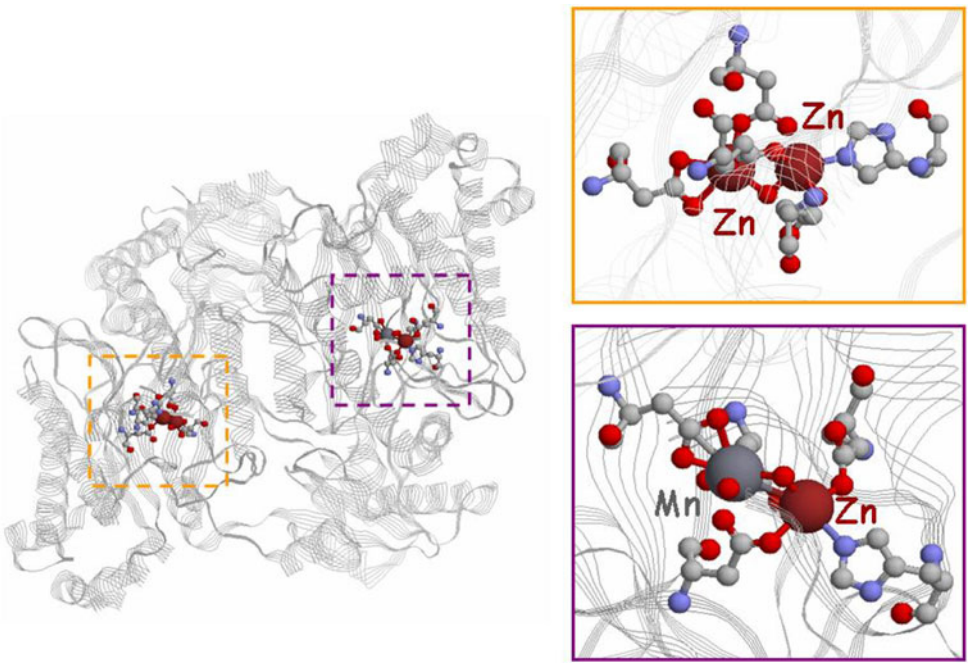

Fig. 6 A cartoon of the geometries of the four prolidase metal binding sites as derived from XAS data analysis

activity if at least one out of the four metal binding sites is occupied by a Mn(II) ion. Furthermore by an accurate analysis of the recently recorded XAS data the atomic structure around each metal binding site has been solved and reconstructed (see Fig. 6 for an artistic view of the atomic environment of the four metal binding sites).

In particular, we have seen that both the recombinant human prolidase preparations we have produced need for protein recovery a preincubation step in the presence of 1 mM $MnCl_2$ prior to the affinity chromatography, thus suggesting that Mn(II) is necessary to allow free access to the N-terminal His tag. At the end of the various purification steps, including the removal of the His tag by on-column Factor-Xa digestion, only one ion per dimer is present at the metal binding sites of the enzyme but this is still enough for partial enzymatic activity (to a level of $\sim$25%).

Our analysis has allowed the identification of the site wherein the purified dimeric enzyme one Mn(II) ion remains bound to the protein, after the successive Mn(II) substitutions by Zn(II) in the other sites. We have identified the site (B2, see Table 2) to which Mn(II) is most tightly bound between the two structurally different B sites (those which are not linked to a His residue, unlike the case of the two identical A1 and A2 sites). We are tempted to relate the affinity difference of the two B sites to the structural difference in the metal coordination modes visible in the PDB crystal structure of human prolidase.

Actually we still do not know whether the presence of Zn(II) ions bound to the high affinity His-related A1 and A2 sites is an artifact of our preparation or whether this also occurs in vivo, not an unrealistic situation as the concentration of Zn(II) is much larger than that of Mn(II). Indeed, one might argue that the presence of heteromeric dinuclear sites is important for in vivo protein activity regulation (Willingham et al. 2001), with Zn(II) having a structural function and Mn(II) a role in promoting protein activity. Further studies in this direction are in progress.

The prolidase from *P. furiosus* is inactive when Zn(II) ions are present in the active sites, but interestingly the substrate specificity of the human and archeon prolidase are significantly different with the human enzyme mainly active against Gly-Pro and the *Pyrococcus* enzyme completely inactive against the same dipeptide (Ghosh et al. 1998).

At the moment there are no firm conclusions about the nature and the number of metal ions in in vivo active human prolidase. It has been recently reported that MetAP from *P. furiosus* can act in vivo as a mononuclear Co(II) or Fe(II) enzyme with the metal ion bound to the high affinity His-related sites (Cosper et al. 2001).

Interestingly at variance with what was described for Pfprol, intestinal prolidases and human recombinant prolidase are not inhibited by incubation with EDTA (O'Cuinn and Fortrell 1975; Yoshimoto et al. 1983; A. Forlino, unpublished data) suggesting a different binding affinity and/or catalytic mechanism for human and Pfprol.

Acknowledgments We wish to thank G.C. Rossi for a careful reading of the manuscript. V. Minicozzi, S. Morante and F. Stellato gratefully acknowledge INFN (Italy) for partial financial support.

Appendix

The EXAFS signal, $\chi(k)$, is defined by the formula

$$\chi(k) = \frac{\mu(k) - \mu_0(k)}{\mu_0(k)}, \tag{4}$$

where $\mu(k)$ is the measured total absorption coefficient and $\mu_0(k)$ is the absorption coefficient of the isolated absorber. k is the wave vector of the extracted electron which is related to the incident photon energy, E, and the ionization energy, E_0, by the obvious relation

$$k = \sqrt{\frac{2m(E - E_0)}{\hbar^2}}, \tag{5}$$

with m the electron mass and $\hbar$ the (reduced) Planck constant.

For the reader's convenience we recall the theoretical formula describing the EXAFS signal. We give it for simplicity in the single scattering approximation which is valid for photon energies sufficiently higher than the threshold energy. Following the standard notation of Boland et al. (1982), it reads

$$\chi(k) = S_0^2 \sum_l \frac{N_l}{k r_l^2} |f_l(k,\pi)| \sin(2kr_l + \varphi_l(k)) \mathrm{e}^{-2\sigma_l^2 k^2} \mathrm{e}^{-2r_l/\lambda(k)}, \tag{6}$$

where the sum runs over the different coordination shells around the absorber. N_l is the number of scatterers of the l-th shell, located at a distance r_l from the absorber and σ_l^2 is the Debye–Waller factor. $|f_l(k,\pi)|$ is the modulus of the back-scattering amplitude and $\phi_l(k)$ the total scattering phase. S_0^2 is an empirical quantity that accounts for all the many-body losses in photo-absorption processes and $\lambda(k)$ is the photo-electron mean free path. In cases where also MS processes become important a formally similar expression holds in which, however, r_l represents the length of the full MS path. Modulus and phase functions are in this case rather complicated expressions which depend on all the scattering events occurring along the MS path (see Lee and Pendry 1975; Benfatto et al. 1986; Gurman et al. 1986; Koningsberger and Prins 1988; Rehr and Albers 1990).

The quantitative analysis of the structural EXAFS signals is performed with the help of the FITEXA code, developed by one of the authors (C. Meneghini).[4] FITEXA exploits the FEFF8.2 package (Zabinsky et al. 1995) for the calculation of backscattering amplitudes, total phase shifts and photoelectron mean free path. Best fit is achieved by minimizing the quantity

$$\xi^2 = \frac{1}{N_\mathrm{p}} \sum_{i=1}^{N_\mathrm{p}} \left[k_i(\chi_\mathrm{exp}(k_i) - \chi_\mathrm{th}(k_i)\right]^2, \tag{7}$$

where χ_exp and χ_th are the experimental and theoretical data, respectively, and the sum is over the number, N_p, of the values of k at which data were collected. The MINUIT (James 1994) subroutine of CERN library is used for data refinement and statistical error analysis.

The fit quality is measured by the associated R^2-factor defined by the formula[5]

$$R^2 = 100 \frac{N_\mathrm{p} \xi^2}{W_0^2} \% \text{ with } W_0^2 = \sum_i \left[k_i \chi_\mathrm{exp}(k_i)\right]^2 \tag{8}$$

A value of R^2 of about 10% is to be considered satisfactory for complex biological molecules.

References

Benfatto M, Natoli CR, Bianconi A, Garcia J, Marcelli A, Fanfoni M, Davoli I (1986) Multiple-scattering regime and higher-order correlations in X-ray-absorption spectra of liquid solutions. Phys Rev B 34:5774–5781. doi:10.1103/PhysRevB.34.5774

Berman HM, Westbrook J, Feng Z, Gilliland G, Bhat TN, Weissig H, Shindyalov IN, Bourne PE (2000) The Protein Data Bank. Nucleic Acids Res 28:235–242. doi:10.1093/nar/28.1.235

Bianconi A, Congiu-Castellano A, Dell'Ariccia M, Giovannelli A, Morante S, Burattini E, Durham PJ (1986) Local Fe site structure in the tense-to-relaxed transition in carp deoxyhemoglobin: a XANES (X-ray absorption near edge structure) study. Proc Natl Acad Sci USA 83:7736–7740. doi:10.1073/pnas.83.20.7736

Boland JJ, Crane SE, Baldeschwieler JD (1982) Theory of extended X-ray absorption fine structure: single and multiple scattering formalisms. J Chem Phys 77:142–153. doi:10.1063/1.443662

Browne P, O'Cuinn G (1983) The purification and characterization of a proline dipeptidase from guinea pig brain. J Biol Chem 258:6147–6154

Chinard FP (1952) Photometric estimation of praline and ornithine. J Biol Chem 199:91–95

Cosper NJ, D'souza VM, Scott RA, Holz RC (2001) Structural evidence that the methionyl aminopeptidase from *Escherichia coli* is a mononuclear metalloprotease. Biochemistry 40:13302–13309. doi:10.1021/bi010837m

Cunningham DF, O'Connor B (1997) Proline specific peptidases. Biochim Biophys Acta 1343:160–186

D'souza VM, Bennet B, Copik AJ, Holz RC (2000) Divalent metal binding properties of the methionyl aminopeptidase from *Escherichia coli*. Biochemistry 39:3817–3826. doi:10.1021/bi9925827

Du X, Tove S, Kast-Hutcheson K, Grunden AM (2005) Characterization of the dinuclear metal center of *Pyrococcus furiosus* prolidase by analysis of targeted mutants. FEBS Lett 579:6140–6146. doi:10.1016/j.febslet.2005.09.086

Fernandez-Espla MD, Martin-Hernandez MC, Fox PF (1997) Purification and characterization of a prolidase from *Lactobacillus*

[4] See the web site: http://webusers.fis.uniroma3.it/~meneghini/. For recent application see (Maret et al. 2005).

[5] See Error Reporting Recommendations: A Report of the Standards and Criteria Committee (2002), URL http://ixs.csrri.iit.edu/

casei subsp. *casei* IFPL 731. Appl Environ Microbiol 63:314–316

Fujii M, Nagaoka Y, Imamura S, Shimizu T (1996) Purification and characterization of a prolidase from *Aureobacterium esteraromaticum*. Biosci Biotechnol Biochem 60:1118–1122

Ghosh M, Grunden AM, Dunn DM, Weiss R, Adams MW (1998) Characterization of native and recombinant forms of an unusual cobalt-dependent proline dipeptidase (prolidase) from the hyperthermophilic archaeon *Pyrococcus furiosus*. J Bacteriol 180:4781–4789

Gurman SJ, Binsted N, Ross I (1986) A rapid, exact, curved-wave theory for EXAFS calculations II. The multiple-scattering contributions. J Phys Chem 19:1845–1861

James F (1994) MINUIT: function minimization and error analysis reference manual version 94.1, CERN Program Library D506

Kobayashi M, Shimizu S (1999) Cobalt proteins. Eur J Biochem 261:1–9. doi:10.1046/j.1432-1327.1999.00186.x

Koningsberger DC, Prins R (eds) (1988) X-ray absorption. Principles, applications, techniques of EXAFS, SEXAFS and XANES. Wiley, New York

Korbas M, Fulla Marsa D, Meyer-Klaucke W (2006) KEMP: a program script for automated biological X-ray absorption spectroscopy data reduction. Rev Sci Instrum 77:063105. doi:10.1063/1.2209954

Lee PA, Pendry JB (1975) Theory of the extended X-ray absorption fine structure. Phys Rev B 11:2795–2811. doi:10.1103/PhysRevB.11.2795

Lowry OH, Rosebrough NJ, Farr AL, Randall RJ (1951) Protein measurement with the folin phenol reagent. J Biol Chem 193:265–275

Lowther WT, Matthews BW (2002) Metalloaminopeptidases: common functional themes in disparate structural surroundings. Chem Rev 102:4581–4608. doi:10.1021/cr0101757

Lupi A, Della Torre S, Campari E, Tenni R, Cetta G, Rossi A, Forlino A (2006) Human recombinant prolidase from eukaryotic and prokaryotic sources Expression, purification, characterization and long-term stability studies. FEBS J 273:5466–5478. doi:10.1111/j.1742-4658.2006.05538.x

Lupi A, Tenni R, Rossi A, Cetta G, Forlino A (2008) Human prolidase and prolidase deficiency: an overview on the characterization of the enzyme involved in proline recycling and on the effects of its mutations. Amino Acids 35:739–752. doi:10.1007/s00726-008-0055-4

Maher MJ, Ghosh M, Grunden AM, Menon AL, Adams MW, Freeman HC, Guss JM (2004) Structure of the prolidase from *Pyrococcus furiosus*. Biochemistry 43:2771–2783. doi:10.1021/bi0356451

Maret M, Bley F, Meneghini C, Albrecht M, Khler J, Bucher E, Hazemann JL (2005) The Cr local structure in epitaxial CrPt3(111) films probed using polarized X-ray absorption fine structure. J Phys Condens Matter 17:2529–2541. doi:10.1088/0953-8984/17/17/001

Meneghini C, Morante S (1998) The active site structure of tetanus neurotoxin resolved by multiple scattering analysis in X-ray absorption spectroscopy. Biophys J 75:1953–1963. doi:10.1016/S0006-3495(98)77636-2

Myara I, Charpentier C, Lemonnier A (1982) Optimal conditions for prolidase assay by proline calorimetric determination: application to iminodipeptiduria. Clin Chim Acta 125:193–205. doi:10.1016/0009-8981(82)90196-6

O'Cuinn G, Fortrell PF (1975) Purification and characterization of an aminoacyl proline hydrolase from guinea-pig intestinal mucosa. Biochim Biophys Acta 391:388–395

Ravel B, Newville M (2005) ATHENA, ARTEMIS, HEPHAESTUS: data analysis for X-ray absorption spectroscopy using IFEFFIT. J Sync Rad 12:537–541. doi:10.1107/S0909049505012719

Rehr JJ, Albers RC (1990) Scattering-matrix formulation of curved-wave multiple-scattering theory: application to X-ray-absorption fine structure. Phys Rev B 41:8139–8149. doi:10.1103/PhysRevB.41.8139

Roderick SL, Matthews BW (1993) Structure of the cobalt-dependent methionine aminopeptidase from *Escherichia coli*: a new type of proteolytic enzyme. Biochemistry 32:3907–3912. doi:10.1021/bi00066a009

Royce PM, Steinmann B (2002) Prolidase deficiency. In: Royce PM, Steinmann B (eds) Connective tissue and its heritable disorders. Wiley-Liss, New York

Tahirov TH, Oki H, Tsukihara T, Ogasahara K, Yutani K, Ogata K, Izu Y, Tsunasawa S, Kato I (1998) Crystal structure of methionine aminopeptidase from hyperthermophile, *Pyrococcus furiosus*. J Mol Biol 284:101–124. doi:10.1006/jmbi.1998.2146

Teo BK, Lee PA (1979) Ab initio calculations of amplitude and phase functions for extended X-ray absorption fine structure spectroscopy. J Am Chem Soc 101:2815–2832. doi:10.1021/ja00505a003

Yang SI, Tanaka T (2008) Characterization of recombinant prolidase from *Lactococcus lactis*—changes in substrate specificity by metal cations and allosteric behaviour of the peptides. FEBS J 275:271–280. doi:10.1111/j.1742-4658.2008.06344.x

Yoshimoto T, Matsubara F, Kawano E, Tsuru D (1983) Prolidase from bovine intestine: purification and characterization. J Biochem 94:1889–1896

Wilcox DE (1996) Binuclear metallohydrolases. Chem Rev 96:2435–2458. doi:10.1021/cr950043b

Willingham K, Maher MJ, Grunden AM, Ghosh M, Adams MW, Freeman HC, Guss JM (2001) Crystallization and characterization of the prolidase from *Pyrococcus furiosus*. Acta Crystallogr D Biol Crystallogr 57:428–430. doi:10.1107/S0907444900020187

Zabinsky SI, Rehr JJ, Ankudinov A, Albers RC, Eller MJ (1995) Multiple scattering calculations of X-ray absorption spectra. Phys Rev B 52:2995–3009. doi:10.1103/PhysRevB.52.2995